1 Global spatially-distributed sectoral GDP map for disaster risk

2 analysis

- 3 Takeshi Shoji^{1,2}, Kiyoharu Kajiyama², Dai Yamazaki^{1,2}, Yuki Kita^{2,3}, Megumi Watanabe^{2,4}
- 4 ¹Graduate School of Engineering, The University of Tokyo, Tokyo, 113-8656, Japan
- ⁵ Institute of Industrial Science, The University of Tokyo, Tokyo, 153-8505, Japan
- 6 ³Gaia Vision Inc., Tokyo, Japan
- 7 ⁴LERMA, Observatoire de Paris, Paris, 75014, France
- 8 Correspondence to: Takeshi Shoji (tshoji@rainbow.iis.u-tokyo.ac.jp)
- 9 Abstract. Global risk assessments of economic losses by natural disasters while considering various land uses is essential.
- 10 However, sector-specific, high-resolution pixel-level economic data are not yet available globally to assess exposure to local
- 11 disasters such as floods. In this study, we employed new land-use data to construct global, spatially distributed map of
- 12 sector-specific gross domestic product (GDP). We developed three global GDP maps, SectGDP30, in 2010, 2015, and 2020
- 13 for service, industry, and agriculture sector with 30 arcsec resolution. The map (SectGDP30) demonstrates strong
- 14 consistency ($R^2 > 0.9$) with actual sub-national statistical data, exhibiting superior alignment compared to conventional
- 15 GDP maps (PB-method) reliant solely on gridded population information. The methodology refined GDP distribution for
- 16 specific sectors. Industry GDP was more accurately mapped using non-residential land areas as a proxy, effectively capturing
- 17 its localized concentrations. Agriculture GDP's accuracy improved by incorporating cropland data and a distance-based
- 18 distribution assumption from population agglomeration. Application of this dataset in estimating flood-induced business
- 19 interruption (BI) losses confirmed the map's capacity to represent inter-sectoral differences in estimated losses, reflecting
- 20 varied hazard spatial distributions. This underscores the importance of considering sector-specific spatial patterns for
- 21 accurate disaster damage assessment. These maps serve as a foundational tool for estimating detailed, sector-classified
- 22 economic losses, enabling precise calculation of sector-specific impacts from diverse natural disasters worldwide. These
- 23 global sectoral GDP maps (SectGDP30) are available at https://doi.org/10.5281/zenodo.15774017 (Shoji et al., 2025).

24 1 Introduction

- 25 In recent years, as natural disasters have become more frequent and found throughout the world (IPCC, 2012), global spatial
- 26 data including land use and socioeconomic information have become essential for estimating the extent of disaster damage
- 27 and losses. With the increasing frequency and impact of localized natural disasters such as floods, high-resolution data

28 capturing the spatial distribution of socioeconomic factors are essential. However, socioeconomic data published by 29 international organizations such as the World Bank are often available only at the national or large municipal level. At the 30 research level, economic data at the municipal level have been studied (Wenz et al., 2023); however, obtaining grid-level data at a resolution of several kilometers has been still challenging.

32

33 For example, as for the impact-assessment of flood disasters, researchers have undertaken a series of studies by spatially 34 calculating the amount of asset quantity and production activity overlapped with inundated areas, leveraging global maps. 35 Achieving this necessitates the downscaling of national-level data of economic activity, mainly gross domestic product 36 (GDP), to finer subnational or grid-based levels. This type of product by downscaling GDP is called a "spatially distributed 37 GDP map". This downscaling practice typically relies on gridded population data (Tanoue et al., 2021; Willner et al., 2018). 38 Alternatively, it has involved the assembly and interpolation of available subnational statistics (Duan et al., 2022; Kummu et 39 al., 2018) or the assumption that average building heights correlate with economic activity intensity (Taguchi et al., 2022). 40 GDP maps developed using these methods are generally created for specific purposes, such as disaster damage estimation, 41 and are therefore not typically released as standalone datasets or products. Among those that are publicly available, 42 "Downscaled gridded global dataset for gross domestic product (GDP) per capita PPP over 1990–2022" by Kummu et al. (2025), is notable. This dataset generates gridded GDP map products with resolutions ranging from 30 arcmin to 30 arcsec 44 for each year since 1990, based on sub-national statistics released by various countries and utilizing population count maps.

45

46 While these studies estimated the total amount of economic losses without considering the difference between sectors, the 47 sector-classified economic losses also need to be estimated because indirect economic losses, such as global supply chain 48 impact caused by the stoppage of production activity (Willner et al., 2018), can vary significantly depending upon the sector 49 directly affected by the flood (Sieg et al., 2019). However, spatial data of sectors by downscaling national-level data have 50 been lacking. Consequently, in the context of global studies, the estimation of sector-specific losses was achieved by 51 extrapolating the values of sectoral occupation fractions within urban area grids, as reported in the European Union, to other 52 regions (Alfieri et al., 2016; Dottori et al., 2018). Alternatively, it is assumed that specific groups of sectors experience 53 uniform damage ratios (Willner et al., 2018; Tanoue et al., 2020). These methods did not consider the different spatial 54 accumulation between each sector and each region, which could lead to the misestimation of sector-classified losses 55 (Jongman et al., 2012; Willner et al., 2018).

56

57 The dearth of global spatial data of the economic sector arises from the absence of worldwide maps with comprehensive land 58 use categorizations (Wenz and Willner, 2022). While regional maps provide sectoral land use classifications, including 59 commercial and industrial areas within urban regions (e.g., European Environmental Agency, 2017; Theobald, 2014; De 60 Moel H et al., 2014; MLIT 2021), these classifications are conspicuously absent from global maps (e.g., Bontemps et al.,

61 2011; Esch et al., 2017). Here we focused on the recent emergence of a global land use map featuring detailed urban area classifications (Pesaresi and Politis, 2022). This development is made possible by the application of machine learning techniques that extrapolate relationships between satellite observations and actual land uses, a methodology initially established by the data in the European Union and the United States (European Environmental Agency, 2017; Theobald, 2014) and subsequently extended to a global scale. Although this dataset facilitates a comprehensive consideration of detailed land-use patterns within urban areas worldwide, no study has yet integrated this dataset with socioeconomic data. Such integration holds the potential to pioneer a novel approach to estimating natural disaster damage accurately with sectoral classifications.

69

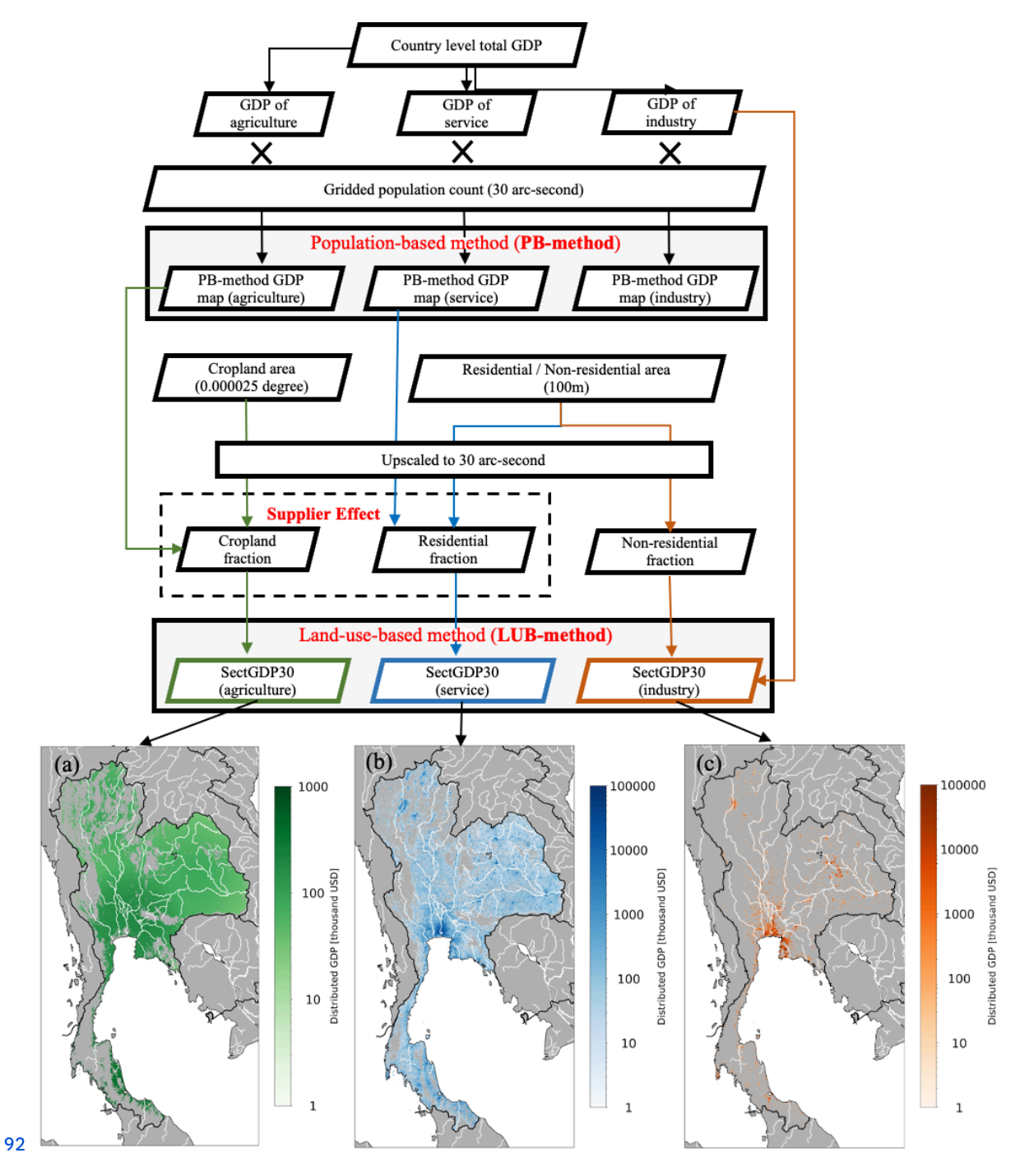
70 The objective of this study is to leverage a recently available global detailed land use map dataset to construct a spatially 1 distributed sectoral GDP map (SectGDP30). The accuracy of the GDP mapping of SectGDP30 is evaluated using global 1 sub-national scale statistics from DOSE dataset (Wenz et al., 2023). Furthermore, to discuss the applicability of SectGDP30 for practical economic loss estimation, this study examines the estimation of business interruption losses incurred due to a 1 flood event in Thailand and compares these estimations with reported values.

75 2 Methods

76 2.1 Spatially distributed sectoral GDP map

The spatially distributed sectoral GDP map was created in two steps (Figure 1). First, we classified country level GDP data 18 into three sectors: the agriculture, service, and industry sector, and they are downscaled to a spatial resolution of 30 arcsec phased on population data, referred as population-based map (PB-method). Second, downscaled estimates are reallocated to the corresponding land use fraction maps derived from satellite products, referred to as land-use-based map (LUB-method). The probability of the agriculture and service sectors, we generated PB-method and subsequently reallocated them using land-use data. This two-step allocation is necessary because GDP is generally correlated with population distribution (Chen et al., 2022; Kummu et al., 2025), and service-sector GDP, in particular, is strongly influenced by urban agglomeration effects (Morikawa, 2011). However, previous studies have shown that at high spatial resolutions, population data alone may not adequately preserve these correlations (Murakami and Yamagata, 2019; Ru et al., 2023). Therefore, integrating land-use information is essential to ensure spatial consistency. Unlike the agriculture and service sectors, industry sector GDP doesn't necessarily follow population distribution. It often expands into suburban or rural areas with low population density (Zhuang and Ye, 2023). Accordingly, we bypass the PB-method step and directly allocate country-level industrial GDP to land use data. The List of the datasets used in this method is shown in Table 1.

90



93 Figure 1: Flowchart of (top) data processing and (bottom) creation of spatial distributed gross domestic product (GDP) maps of 94 Thailand for the (a) service, (b) industrial, and (c) agricultural sectors.

Data	Format	Datatype	Values range	Spatial resolution	Temporal resolution	Data source, Reference
Built up surface area						Child I I was Carlowed I was
Non-residential surface area	Raster	UInt16	0-10000	100m	five years interval (1975-2020)	Global Human Settlement Layer (Pesaresi and Politis, 2022)
Crop land area	Raster	Boolean	0,1 (0 - no croplands, 1 - croplands)	0.9 arcsec	five years interval (2003-2019)	Potapov et al., 2022
Population count	Raster	Float64	0-Inf	30arcsec	five years interval (1975-2020)	Global Human Settlement Layer (Pesaresi and Politis, 2022)
Administrative units	Vector (Polygon)	-	-	-	-	GADM 4.1 (2023) Level 1 Layer

95 96

97 Table 1: List of the datasets used in this study.

98 2.1.1 Population-based sectoral GDP

99 In the first step, country-level GDP was partitioned into three sectors and then spatially distributed in proportion to population data at a 100 spatial resolution of 30 arcsec. We used GDP data published by the World Bank (2023), which includes both annual GDP values and their 101 sectoral ratios for the service, industrial, and agricultural sectors, and the Global Human Settlement Layer (GHSL) population grid 102 (R2023; Pesaresi and Politis, 2022) as the source of the global gridded population map. The definition of each sector is shown in Table 2. 103 This downscaling method has been widely employed in previous studies (Kummu et al., 2018; Murakami and Yamagata, 2019) and will be 104 utilized in a later section for comparison with the new method proposed in this study.

105 2.1.2 Sectoral land use fraction map

106 In the second, step, we reallocated PB-method to global sectoral land use fraction map. We generated a sectoral land use 107 fraction map classified into three sectors (service, industry, and agriculture) and three land use type maps with different 108 spatial resolutions: residential (RES), non-residential (NRES), and cropland (CROP). To distinguish RES and NRES areas, 109 we used Global Human Settlement Layer (GHSL) (Pesaresi and Politis, 2022) built-up surface (R2022) data. This layer has 110 100 × 100 m resolution; each pixel has a value of 0-10,000 m2 and residential or non-residential areas may be present within 111 one pixel. For the CROP area, we used the global map of cropland extent (Potapov et al., 2022), provided by Global Land 112 Analysis & Discovery, which has a global spatial resolution of 0.9 arcsec. Maps with the three classes were resampled and 113 combined into a single global sectoral land use (residential, non-residential, and cropland) fraction map at 30 arcsec 114 resolution.

115

116 First, we upscaled the land use maps and simultaneously converted the value of each pixel in both maps into the sectoral 117 fraction within one pixel. In each pixel, RES and NRES had values of 0–10000 m2 and CROP had a value of 0 or 1 (not 118 cropland or cropland). We upscaled the land use maps to 30 arcsec resolution from RES and NRES at a resolution of 100 ×

119 100 m and CROP at a resolution of 0.9 arcsec using the GDAL averaging method (GDAL/OGR contributors. 2024). Using

120 the 30 arcsec maps, we calculated the area attributed to each land use type in one pixel with a size of 1 × 1 arcsec and

121 obtained land use fractions for each pixel. Because RES/NRES and CROP had different data sources, the total of the three

122 land use type fractions was greater than one in some pixels. Therefore, we assumed that the CROP fraction could fill only

123 areas that were not designated as RES or NRES. Under this assumption, we modified the CROP fraction in each pixel as

124 follows:

$$125 \ MCROP_{i} = min(CROP_{i}, (1 - RES_{i} - NRES_{i}))$$

$$(1)$$

126 where MCROP, is the modified CROP fraction in pixel i, CROP, is the original CROP fraction, RES, is the RES fraction,

127 and NRES, is the NRES fraction.

128 After this modification, RES, NRES, and MCROP were considered to represent the service, industrial, and agricultural land

129 use sectors, respectively.

130 2.1.3 Land-use-based agriculture sector GDP

131 To better reflect the spatial structure of production activities, we introduce the supplier effect, which assumes a

132 beneficiary-supplier relationship. Specifically, agricultural production occurring in peri-urban or rural areas surrounding

133 major population centers is regarded as supplying food and resources to those urban beneficiaries. These agricultural zones,

134 while themselves sparsely populated, are functionally integrated with the urban economy. Therefore, they are expected to

135 exhibit higher GDP values than similarly sparse regions that are not spatially or economically connected to urban demand.

136 To capture this spatial interdependence, the supplier effect applies a distance-decay reallocation from beneficiary pixels in

137 PB-method to nearby supply-side pixels, namely those identified as MCROP. Technically, this is implemented as a linear

138 decay function, in which full weight is given within an inner threshold of 150 km, and weight decrease linearly to zero at an

139 outer threshold of 300km.

140
$$w_{ij} = if d_{ij} \le d_{in}$$
: 1; $if d_{in} < d_{ij} \le d_{out}$: $1 - (d_{ij} - d_{in}) / d_{in}$; $if d_{ij} > d_{out}$: 0 (2)

141

Sector	Definition of ISIC		
Agriculture	ISIC 01-03 (A)		
Service*	ISIC 50-99		
Industry	ISIC 05-43 (B-F)		

*Noted that only the Service sector is based on ISIC Rev. 3.

143 Table 2: Definition of each sector, based on the International Standard Industrial Classification (ISIC) Rev 4, in the 144 GDP data by the World Bank (2023).

145 2.1.4 Land-use-based service sector GDP

146 Similarly, PB-method of the service sector is reallocated to residential areas (RES) by applying the supplier effect. The 147 rationale here differs slightly from that for agriculture. Grid-scale population data (e.g., at 30 arcsec resolution, or 148 approximately 1 × 1 km per pixel) are too fine to represent realistic service usage, since people commonly travel more than 149 1 km by car or public transportation to access services (Ciccone and Hall, 1996). Therefore, this reallocation is designed to 150 represent commuting patterns, where service activities in peri-urban zones support nearby urban demand centers. In this 151 context, we use a supplier effect with an inner threshold of 25 km (representing high-intensity interaction) and an outer 152 threshold of 50 km, beyond which service contributions are assumed negligible.

153 2.1.5 Land-use-based industry sector GDP

154 We distributed the industry sector GDP in each country by multiplying the distributed GDP per pixel by the NRES in each 155 pixel. Thus, the distribution was performed for each country, as follows:

156 Industry GDP per pixel_{country} = Total Industry GDP_{country} /
$$\sum_{i=1}^{n} NRES_{i}$$
 (3)

157
$$Industry\ GDP_{country,i} = Industry\ GDP\ per\ pixel_{country} \times NRES_i$$
 (4)

158 where is the Industry GDP per pixel of sector s in the country, is the total sectoral GDP of industry in the country, is 159 the non-residential area in pixel i, n is the total number of pixels in the country, and is the distributed industry GDP in 160 pixel i in the country.

161 2.2 Comparison of GDP distribution methods

We created two types of spatial distributed GDP map: population-based (PB-method), Land-use-based (LUB-method). The PB map was generated by downscaling the country GDP only in proportion to the gridded population count into a 30 arcsec map. The LUB-method was generated for each sectoral area and sectoral GDP per area. To assess the effectiveness of the proposed LUB mapping approach, we compared it against PB-method using the DOSE dataset (Wenz et al., 2023), which provides sectoral GDP estimates at the sub-national administrative unit level (GADM level 1). Both GDP maps (i.e., 167 PB-method and LUB-method) were spatially aggregated from 30 arcsec resolution to the corresponding GADM Level 1 administrative boundaries to enable direct comparison with DOSE data. Comparison involved three steps: (1) Scatter plots were generated to evaluate the agreement between the aggregated values from each GDP map and corresponding sectoral

170 GDP values from the DOSE dataset (agriculture, service, and industry) used as reference data. (2) For each method and 171 sector, we computed the absolute value of the relative error between estimated and reference GDP values and derived the 172 cumulative distribution functions to illustrate the distribution of errors across all administrative units. (3) We computed the 173 difference in absolute relative errors between the LUB-method and PB-method to evaluate the improvement or deterioration 174 in accuracy. For each administrative unit, this metric was calculated as:

175
$$\Delta E = E_{LUB} - E_{PB}$$
, where $E = \frac{\left|GDP_{estimate} - GDP_{DOSE}\right|}{GDP_{DOSE}}$ (5)

176 A negative value of (ΔE) indicates that LUB-method is closer to the reference than PB-method (i.e., an improvement), while 177 a positive value indicates a deterioration in accuracy compared to PB-method. The comparison was conducted using only 178 administrative units for which all three sectoral GDP values were available for the year 2010. In total, the comparison 179 included 1,165 administrative units across 57 countries.

180 3 Results

We developed three GDP maps for service, industry, and agriculture sectors in 2010, 2015, and 2020. We excluded other years because of the low coverage of national GDP statistics in the World Bank data. Hereafter, the map generated using the LUB method within the Methods will be referred to as "SectGDP30", and the map generated using the PB method will be referred to as "PB-method". The maps of SectGDP30 are shown in Fig. 2 (a), (b), and (c). Additionally, to clarify the difference of spatial distribution among sectors, we showed (d) the map of the largest GDP sector in each grid in the world. Globally, the distribution of economic sectors generally correlates with population distribution, with concentrations observed in urban centers. However, variations exist in the detailed distributions. The service sector's distribution predominantly concentrates in urban areas across countries, consistent with population distribution patterns and the use of residential data. In contrast, industrial GDP, proxied by non-residential areas, shows a tendency toward greater concentration in coastal regions. Conversely, agricultural GDP, while exhibiting some correlation with population distribution, is characterized by a more expansive distribution in inland areas compared to the service sector.

192

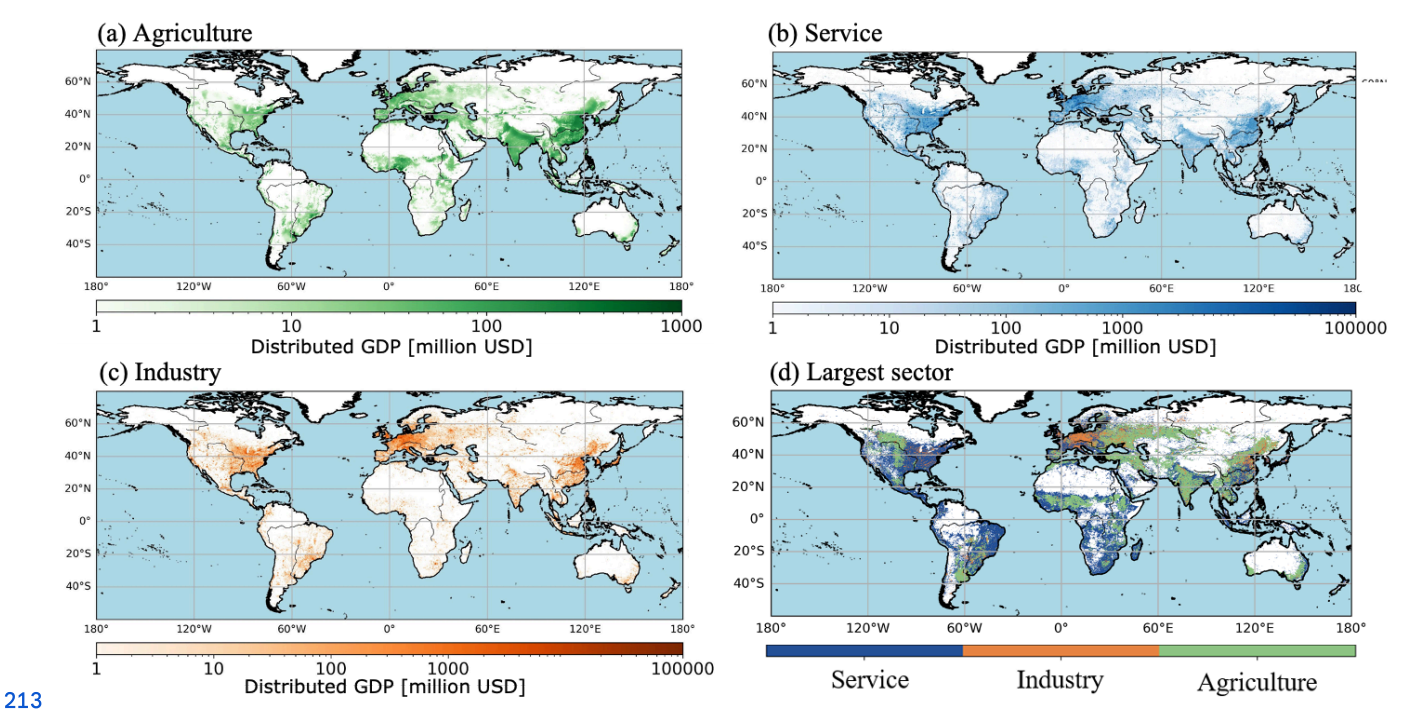
Examining individual countries allows for the identification of more specific differences in the distribution of each sector at 194 a finer scale, shown in Fig. 3. In the figure of Japan, Japan's three major metropolitan areas—Tokyo, Osaka, and 195 Aichi—shows variations in sectoral distribution, despite their common characteristic of high population concentration. In the 196 GDP map, the service sector predominates in the coastal areas of Tokyo and Osaka, which are marked by high population 197 and service industry presence. In contrast, Aichi's coastal regions exhibit a widespread predominance of industrial GDP. 198 Industrial GDP is not uniformly distributed across the entire Aichi area. Within Aichi, the more inland urban center, such as 199 the Nagoya area, shows a prevalence of the service sector, with industrial GDP concentrated in coastal areas. These findings

200 align with Aichi's higher proportion of industrial GDP compared to Tokyo and Osaka (DOSE, 2024), and the formation of an 201 extensive industrial belt along its coastal regions. This dataset facilitates the depiction of detailed distributional differences 202 within these areas.

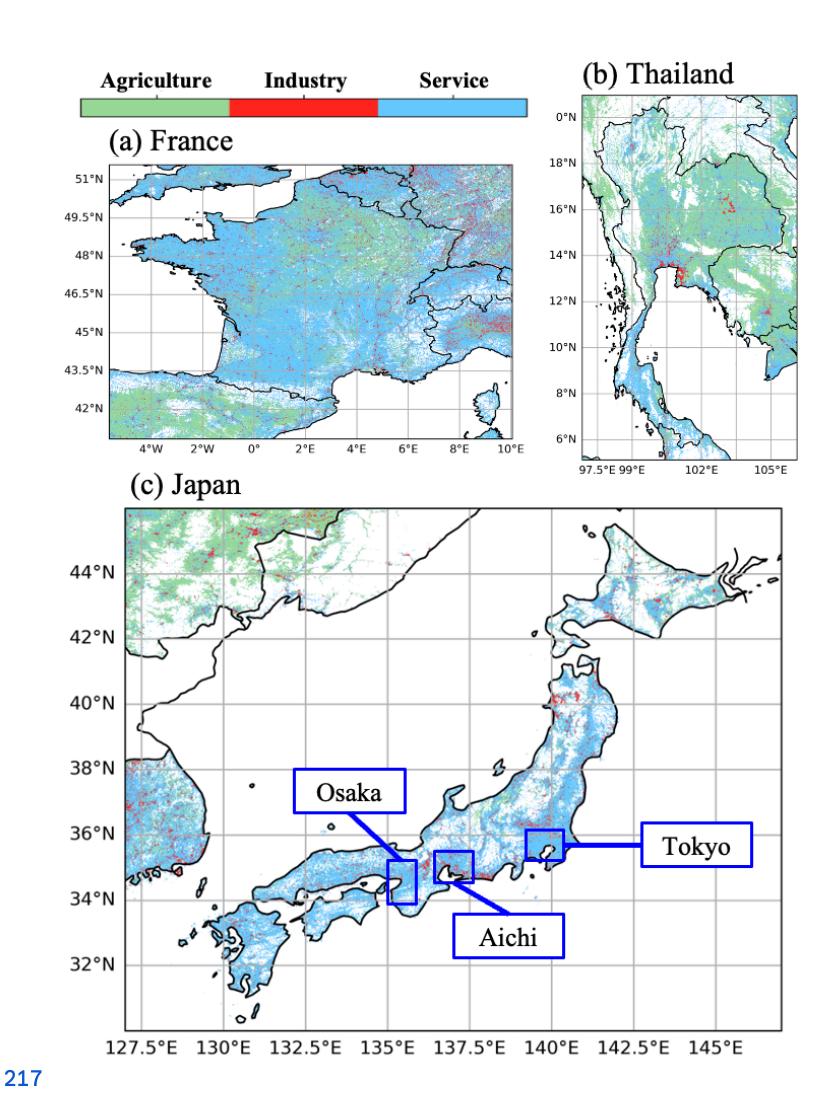
203

When comparing central Bangkok with its southeastern region, a similar pattern emerges as a case in Japan. The southeastern 205 area, specifically the Eastern Seaboard and Eastern Economic Corridor (EEC) centered around Laem Chabang Port, has 206 developed as an industrial hub. In this region, industrial GDP predominates over service sector GDP. Regarding the 207 distribution of agricultural GDP, Japan shows fewer pixels where agricultural GDP is dominant, largely because much of its 208 agricultural land is located relatively close to urban areas. However, in Thailand and France, extensive areas with dominant 209 agricultural GDP are observed around metropolitan centers like Bangkok and Paris. For instance, Figure 4 (a), which shows 210 only agricultural GDP for France, illustrates that agricultural GDP is minimally developed around densely populated Paris. 211 Conversely, it depicts widespread agricultural activity in the less populated surrounding regions.

212



214 Figure 2: The sectoral GDP maps of (a) service sector, (b) industry sector, (c) agricultural sector, (d) the map of the largest GDP 215 sector in each grid of 30 arcsec.



219

224

218 Figure 3: The map of the largest GDP sector in each grid of 30 arcsec in (a) France, (b) Thailand, and (c) Japan.

220 To validate the accuracy of this GDP map, we conducted a comparative analysis with DOSE, a dataset providing sectoral GDP figures at the sub-national administrative unit level. For this validation, the 30 arcsec resolution GDP map was spatially aggregated according to the 222 GADM dataset's Level 1 administrative divisions, which are used by DOSE. The aggregated GDP values for each administrative unit were then calculated and compared with DOSE's figures.

225 The results are presented in Figure 4 (a), (b), and (c). These three scatter plots indicate that SectGDP30 exhibits a similar distribution to 226 actual sub-national scale sectoral GDP ($R^2 > 0.9$ in all the sectors). When examined by sector, many administrative units with 227 discrepancies in service and industrial GDP show an underestimation compared to actual data. Given that the total GDP per sector at the

actional level aligns with real data in this study, this discrepancy likely results from over-distributing GDP in a few administrative units within certain countries, leading to an underestimation in many other smaller administrative units. While service and industrial GDP inherently concentrate in specific local areas, and this GDP map depicts that, some countries show an excessive concentration in particular regions. This trend is less apparent in agricultural GDP, which exhibits less localized distribution, and no strong pattern of overestimation or underestimation was observed.

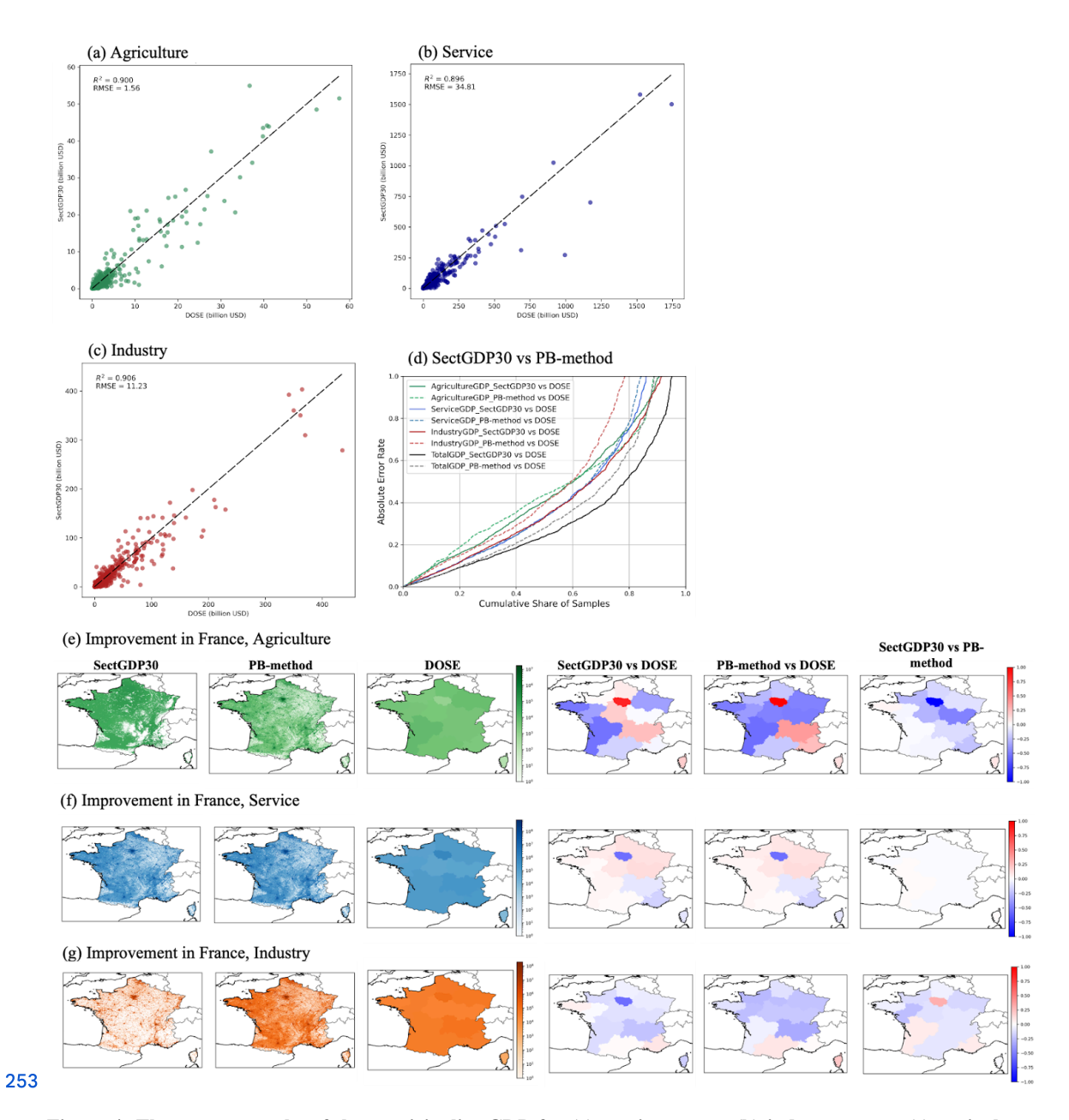
233

Next, we compared the results from SectGDP30 with PB-method. The comparison method involved using sectoral GDP figures for each administrative unit, as before, and calculating the cumulative distribution of the differences from DOSE's figures. This result is presented in Figure 4 (d). Sectoral analysis reveals that the industrial sector shows the most significant improvement when compared to PB-method. As previously mentioned, industrial GDP distribution often exhibits localized concentrations even in sparsely populated areas. This suggests that a method using only non-residential land use information and concentrating distribution over relatively small areas is more appropriate than PB-method, which relies on population distribution data.

240

241 The service sector shows a slight decline in accuracy compared to PB-method. In the service sector, overall regional results showed a 242 slight decrease in accuracy for SectGDP30 compared to PB-method. However, some regions exhibited improved accuracy with 243 SectGDP30. Fundamentally, there is minimal difference between SectGDP30 and PB-method as the spatial distributions of residential 244 areas (upon which SectGDP30 relies) and population (upon which PB-method relies) largely coincide.

245 Conversely, SectGDP30 incorporates Supplier effect, reallocating each grid's GDP to residential areas within a 50km radius. This results in 246 a smoother connection of urban and rural area distribution differences compared to PB-method. This effect is evident in the Alpine regions 247 of Switzerland (CHE), specifically in administrative level districts such as Uri, Wallis, Graubunden, and Glarus. While these Swiss Alpine 248 areas have a significant population, residential areas are limited, and actual statistical service GDP is not high. Therefore, in Switzerland, 249 service GDP should be distributed not based on simple population distribution but rather in the plains north of the Alps, where numerous 250 residential areas exist. This case demonstrated an improvement in SectGDP30 accuracy. Agricultural GDP also shows an improvement 251 compared to PB-method, with an increase in the number of administrative units exhibiting smaller errors.



254 Figure 4: The scatter graphs of the municipality GDP for (a) service sector (b) industry sector (c) agriculture sector and (d) the 255 cumulative distribution of the errors between DOSE and SectGDP30 and between DOSE and PB-method for each sector.

257 4 Discussion - Business interruption loss estimation for the 2011 Thailand flood

258 To assess how the improvement of the GDP map affects the result of flood loss estimation, an additional analysis of estimating business interruption losses resulting from the actual flood event in Thailand in 2011 by the new sectoral GDP 260 map was conducted. Following established definitions of economic losses from prior studies (Tanoue et al., 2020; Rose, 261 2004), economic impacts can be categorized into three main types: damage, direct economic loss, and indirect economic 262 loss. This additional analysis focused exclusively on estimating Business Interruption loss (BI loss) among these three 263 economic impacts due to the lack of information necessary for the estimation of the other components.

264

265 To calculate BI loss, we prepared hazard, exposure, and vulnerability data. As the hazard, we used two inundation period 266 maps of the target event in Thailand, based on simulation and satellite observations. The simulation-based inundation period 267 map was generated using the Catchment-based Macro-scale Floodplain (CaMa-Flood) global riverine inundation model 268 (Yamazaki et al., 2011). To obtain an inundation map based on the simulation by CaMa-Flood, CaMa-Flood used daily 269 runoff data generated by a reduced-bias meteorological forcing dataset at 15-arcmin resolution, and S14FD-Reanalysis data 270 (Iizumi et al., 2017) to simulate the daily inundation depth at 15-min resolution. Because S14FD is a bias-corrected dataset, 271 we used daily inundation depth values without bias correction, such that the inundation period may be calculated directly 272 from the daily inundation depth (Taguchi et al., 2022). Then, we downscaled the 15-arcmin daily inundation depth to 30 arcsec resolution and calculated the inundation period as the number of days in which the inundation depth exceeded 0.5 m 274 in each pixel. We also used an inundation period map based on Terra/Moderate Resolution Imaging Spectroradiometer 275 (MODIS) images, which is publicly available on the Global Flood Database (Tellman et al., 2021). We referred to the former 276 hazard map as "CaMa-Flood" and the latter map as "MODIS" in this study. The days between August and December in 2011 277 were only counted as inundation days for matching the inundation period by CaMa-Flood simulation and that by MODIS 278 observation, which started from August and ended around the end of December.

279

As exposure, we used two spatial distributed GDP maps at 30 arcsec resolution for comparison, SectGDP30 and PB-method. 281 As a vulnerability, we considered a recovery coefficient, which decided the ratio of the length of recovery period which is 282 required until business restart to the inundation period. This value reflects the system vulnerability of the city. We used 2 as a 283 recovery coefficient, which was used in previous study on a global scale (Taguchi et al., 2022). As for the recovery period as 284 vulnerability, we used the method of Tanoue et al. (2020). The recovery period RP_i , when the production in a pixel is 285 assumed to have recovered linearly from zero at the end of the flood period to the same level of production before the flood, 286 was obtained by multiplying the inundation period by a coefficient (= 2 in this study). Thus, the recovery period was 287 assumed to take twice as long as the inundation period. Finally, BI loss was estimated by the method described by Tanoue et 288 al. (2020), as follows:

289 BI loss =
$$\sum_{i=1}^{N} \sum_{s}^{3} \left\{ (IP_i + \frac{RP_i}{2}) \times \frac{AGDP_{i,s}}{Nd} \right\}$$
 (6)

290 where i, N, and s are the pixel number, total number of pixels in the inundated area, and sector number (1 = service, 2 =

291 industry, and 3 = agriculture), respectively; IP_i , RP_i , $AGDP_{i,s}$, and Nd are the inundation period, recovery period at pixel i,

292 annual GDP of pixel i and sector s, and the number of days in a year.

293 And we obtained the total BI losses by summing BI losses of all the grids in the target area.

294

295 The results of the BI loss estimation were shown in Fig. 5. We compared the calculated BI losses with the actual economic

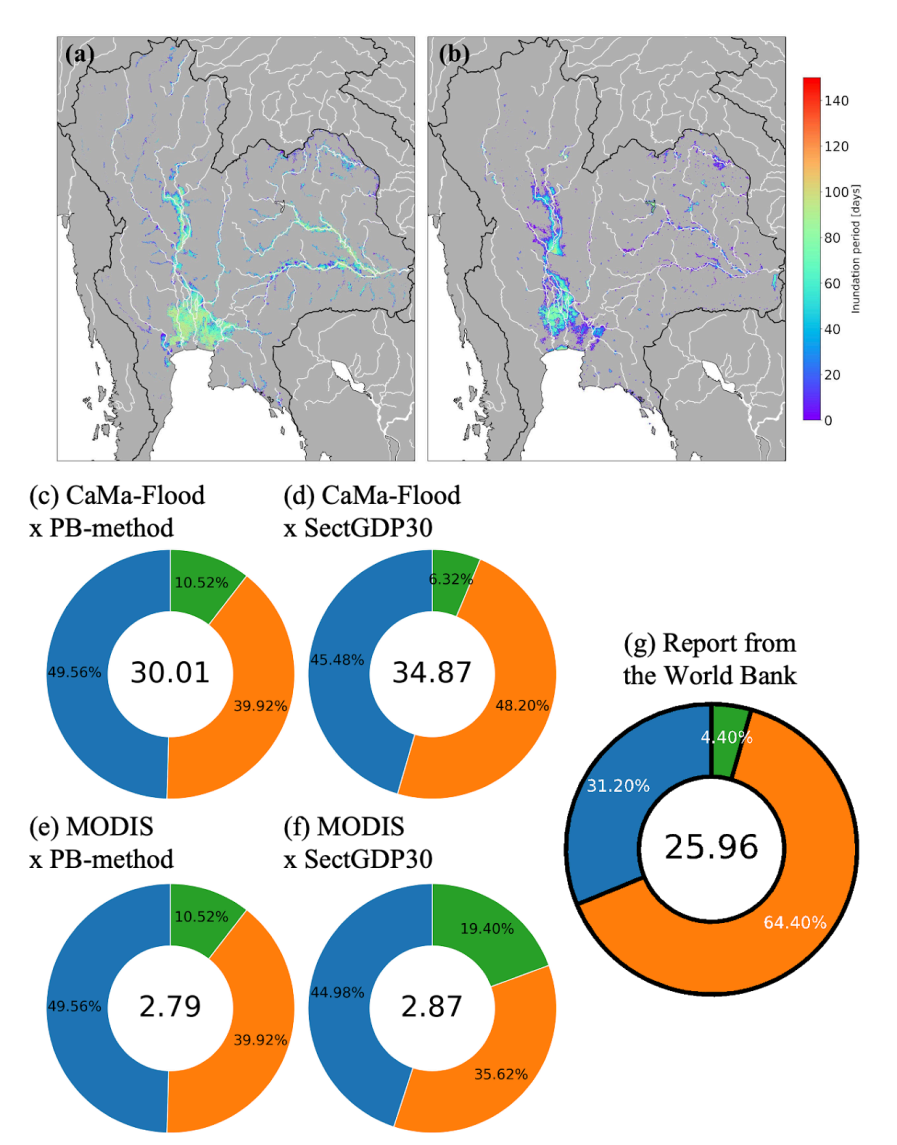
296 loss reported in the PDNA (The World Bank, 2011). In this report, both damage and loss were estimated. Damage is due to

297 the destruction of physical assets and loss is caused by foregone production and income and higher expenditures in the

298 definition in the report. This means that the loss in the report included both business interruption loss and other additional

299 expenditures and costs. Because there was not any other reported loss which only focused on BI loss, we compared with the

300 loss, including other components, in this report.



BI loss [billion USD, current value in 2011]

303 Figure 5: Spatial distribution of the inundation period of the 2011 Thailand flood, obtained from (a) 304 Catchment-based Macro-scale Floodplain (CaMa-Flood) simulation and (b) Moderate Resolution Imaging 305 Spectroradiometer (MODIS) observation data, and the simulation Business interruption losses (USD billion, current 306 value in 2011) due to the 2011 Thailand flood, estimated by combining hazards and exposures; the total loss is written 307 in the center of each circle. (c) CaMa-Flood and PB-method, (d) CaMa-Flood and SectGDP30, (e) MODIS and 308 PB-method, (f) MODIS and SectGDP30, and (g) the World Bank report (2011).

302

310 Firstly, comparing the losses by the different hazard data with the same exposure, SectGDP30, the service sector loss 311 according to CaMa-Flood (USD 15.86 billion) was over 12-fold larger than that according to MODIS (USD 1.29 billion). 312 This large difference was caused by the shorter average inundation period and smaller flood area in MODIS than in 313 CaMa-Flood. MODIS is known to tend to fail to capture the flood extent in urban areas with high densities of tall buildings 314 and that leads to the underestimation in inundation. In addition to different total losses, ratios of industry sector loss to the 315 total loss differed between two results: 48.20% according to CaMa-Flood and 35.62% according to MODIS. This result 316 showed the sectoral ratio of the loss can be changed depending on spatially different hazards. It is caused by the fact that 317 SecGDP30 can show the different spatial distribution of each sectoral GDP, while municipality-level statistics cannot show 318 the spatial distribution in a fine resolution. This sectoral difference was newly found by this study since the traditional 319 population-based GDP map also could not show this difference between sectors.

320

321 Comparing the results using CaMa-Flood and SectGDP30 with the World Bank Report figures (Figure 5 (d) and (g)), 322 SectGDP30 more accurately represents the smaller proportions of agricultural damage compared to when PB-method is used 323 (Figure 5 (c)). This indicates that SectGDP30 can effectively constrain the allocation of agricultural GDP in areas with high 324 population but limited agricultural land. Conversely, while the Report figures show a significant proportion for the industry 325 sector, SectGDP30 results estimate the industry sector to be almost on par with the service sector. It showed the industry loss 326 was underestimated although the hazard in the numerical simulation, by CaMa-Flood, captured the flood extent over the 327 industrial sector area and the long-lasting inundation period. The reported value excludes assets damage but includes 328 economic losses other than production reduction by direct contact with the flood, such as production stoppage due to 329 shortages of raw materials induced by blocked roads. Therefore, if we assume that the new sectoral GDP map captured the 330 industrial locations and they were successfully considered to be flooded, this underestimation is presumed to be caused by a 331 lack of data reflecting the indirect production stoppage.

332

333 Related to this limitation of the indirect production stoppage, it is important to recognize that the methodology, including that
334 of this paper and previous studies, which determines the GDP produced in each pixel using indicators such as GDP per unit
335 area, overlooks the fact that labor supplied from remote locations is necessary for GDP production. To rephrase this with the
336 example of a factory affected by a disaster: while the GDP output itself occurs at the factory's location, the workers who
337 carry out the production reside in surrounding or remote areas. Therefore, if a disaster occurs in these remote residential
338 areas, the GDP output should cease. However, pixel-based calculation methods would fail to represent this cessation of GDP
339 output as long as the factory's pixel is unaffected. This is considered a non-negligible impact in regions where economic
340 activity and residential areas are clearly separated, but quantifying this impact on a global scale is currently challenging.
341 Alongside future research on regional differences in GDP per unit area, this remains a limitation that we must consider
342 moving forward.

343 5 Data availability

- 344 The global sectoral GDP maps are publicly available via Zenodo at https://doi.org/10.5281/zenodo.13991673 (Shoji et al.,
- 345 2024). The maps on Zenodo correspond to the SBCE maps in this paper and are stored as geotiff files. In total, there are nine
- 346 maps in the dataset, for each sector (service, industry, and agriculture) and year (2010, 2015, and 2020).

347 6 Summary

- 348 This study developed a spatially distributed sectoral GDP map (SectGDP30) by leveraging recently available global,
- 349 high-resolution land use datasets. This map demonstrates strong consistency ($R^2 > 0.9$) with actual sub-national statistical
- 350 data and exhibits greater alignment with sub-national GDP statistics compared to conventional GDP maps (PB-method) that
- 351 rely solely on gridded population maps.

352

- 353 For the industry sector, the methodology successfully distributed industrial GDP with better accuracy than population
- 354 distribution alone. This was achieved by adopting "Non-residential areas" as a proxy, which effectively captures the localized
- 355 nature of industrial GDP distribution in specific regions within each country. For agriculture, accuracy was improved over
- 356 PB-method by distributing GDP based on farmland maps and assuming GDP generation in areas approximately 150-300 km
- 357 from wide-area population centers. Regarding the service sector, incorporating population distribution within specific ranges,
- 358 even when using residential land use map information, resulted in GDP being distributed only to actual built-up and
- 359 designated residential areas. This approach achieved an accuracy comparable to PB-method.

360

- 361 As an application of this dataset, business interruption (BI) loss estimation due to floods was conducted using the sectoral
- 362 GDP map. This confirmed that the new sectoral GDP map can represent inter-sectoral differences in estimated BI losses,
- 363 corresponding to varying spatial distributions of hazards. This validation underscores the importance of considering the
- 364 spatially distinct distributions of sectors when estimating actual disaster damage. It also highlights the need for developing
- 365 new estimation methods that account for the processes of GDP generation.

366

- 367 This new global sectoral GDP map serves as a foundational tool for estimating sector-classified economic losses. It
- 368 meticulously considers the complexity of global land use patterns at a detailed level, enabling accurate calculation of
- 369 sector-specific losses from various natural disasters on a global scale.

370

372 Competing interests

373 The contact author has declared that none of the authors has any competing interests.

374

375 Acknowledgement

- 376 This work was supported by Japan Science and Technology Agency (JST) [Moonshot R&D; JPMJMS2281] and Ministry of
- 377 the Environment of Japan / Environmental Restoration and Conservation Agency [Development Fund;
- 378 JPMEERF23S21130].

379

380 References

- 381 Alfieri L, Bisselink B, Dottori F, Naumann G, De Roo A, Salamon P, Wyser K, Feyen L.: Global projections of river flood
- **382** risk in a warmer world. Earth's Future 5: 171-182, 2017.
- 383 Bontemps S, Herold M, Kooistra L, Van Groenestijn A, Hartley A, Arino O, Moreau I, Defourny P.: Revisiting land cover
- 384 observations to address the needs of the climate modelling community. Earth System Science/Response to Global Change:
- 385 Climate Change, Preprint Report, 2011.
- 386 Chen, J., Gao, M., Cheng, S., Hou, W., Song, M., Liu, X., & Liu, Y.: Global 1 km× 1 km gridded revised real gross domestic
- 387 product and electricity consumption during 1992–2019 based on calibrated nighttime light data. Scientific Data, 9(1), 202,
- **388** 2022.
- 389 Ciccone A, Hall RE.: Productivity and the density of economic activity. The American Economic Review 86: 54-70.
- 390 http://www.jstor.org/stable/2118255, 1996.
- 391 CIESIN (Center for International Earth Science Information Network).: Global Rural-Urban Mapping Project, Version 1
- 392 (GRUMPv1): Urban Extent Polygons, v1.02, 2011.
- 393 De Moel H, Van Vliet M, Aerts JCJH.: Evaluating the effect of flood damage-reducing measures: a case study of the
- 394 unembanked area of Rotterdam, the Netherlands. Regional Environmental Change 14: 895–908, 2014.
- 395 Dottori F, Szewczyk W, Ciscar J, Zhao F, Alfieri L, Hirabayashi Y, Bianchi A, Mongelli I, Frieler K, Betts RA, Feyen L.:
- 396 Increased human and economic losses from river flooding with anthropogenic warming. Nature Climate Change 8: 781-786,
- **397** 2018.
- 398 Duan Y, Xiong J, Cheng W, Li Y, Wang N, Shen G, Yang J.: Increasing Global Flood Risk in 2005–2020 from a Multi-Scale
- 399 Perspective. Remote Sensing 14: 5551, 2022.

- 400 Esch T, Heldens W, Hirner A, Keil M, Marconcini M, Roth A, Zeidler J, Dech S, Strano E.: Breaking new ground in
- 401 mapping human settlements from space The Global Urban Footprint. ISPRS Journal of Photogrammetry and Remote
- 402 Sensing 134: 30-42, 2017.
- 403 GADM 4.1. https://gadm.org/.
- 404 GDAL/OGR contributors.: GDAL/OGR Geospatial Data Abstraction software Library. Open Source Geospatial Foundation.
- 405 https://gdal.org, 2024.
- 406 Hirabayashi Y, Mahendran R, Koirala S, Konoshima L, Yamazaki D, Watanabe S, Kim H, Kanae S.: Global flood risk under
- 407 climate change. Nature climate change 3: 816-821, 2013.
- 408 Huizinga J, De Moel H, Szewczyk W.: Global flood depth-damage functions: methodology and the database with guidelines.
- 409 European Commission, Joint Research Centre, 2016.
- 410 Iizumi T, Takikawa H, Hirabayashi Y, Hanasaki N, Nishimori M.: Contributions of different bias-correction methods and
- 411 reference meteorological forcing data sets to uncertainty in projected temperature and precipitation extremes. Journal of
- **412** Geophysical Research-Atmospheres, 2017.
- 413 IMF.: How Should We Measure City Size Theory and Evidence Within and Across Rich and Poor Countries. IMF:
- 414 Washington, DC, USA.
- 415 https://www.imf.org/en/Publications/WP/Issues/2019/09/20/How-Should-We-Measure-City-Size-Theory-and-Evidence-With
- 416 in-and-Across-Rich-and-Poor-Countries-48671, 2019.
- 417 Inoue S.: Agriculture and its Policy in Thailand. MAFF (Ministry of Agriculture, Forestry and Fisheries).
- 418 https://www.maff.go.jp/primaff/koho/seminar/2010/attach/pdf/101026_01.pdf. (In Japanese), 2010.
- 419 IPCC.: Managing the Risks of Extreme Events and Disasters to Advance Climate Change Adaptation. A Special Report of
- 420 Working Groups I and II of the Intergovernmental Panel on Climate Change: 582 pp, 2012.
- 421 Jongman B, Kreibich H, Apel H, Barredo JI, Bates PD, Feyen L, Gericke A, Neal J, Aerts JCJH, Ward PJ.: Natural Hazards
- 422 and Earth System Sciences 12: 3733-3752, 2012.
- 423 Jovel RJ, Mudahar M.: Damage, loss, and needs assessment guidance notes: Volume 3. Estimation of post-disaster needs for
- 424 recovery and reconstruction. Washington, DC, Report. http://hdl.handle.net/10986/19046, 2010.
- 425 Kimura S, Ishikawa Y, Katada T, Asano K, Sato H.: The structural analysis of economic damage of offices by flood disasters
- 426 in urban areas. Japanese Journal of JSCE 63: 88-100 (in Japanese), 2007.
- 427 Koks EE, Bočkarjova M, De Moel H, Aerts JCJH.: Integrated Direct and Indirect Flood Risk Modeling: Development and
- 428 Sensitivity Analysis: Integrated Direct and Indirect Flood Risk Modeling, Risk Analysis 35: 882-900, 2015.
- 429 Kummu M, Maija T, Guillaume JHA.: Gridded global datasets for gross domestic product and human development index
- 430 over 1990–2015. Scientific Data 5: 180004, 2018.
- 431 Kummu, M., Kosonen, M., & Masoumzadeh Sayyar, S.: Downscaled gridded global dataset for gross domestic product
- **432** (GDP) per capita PPP over 1990–2022. Scientific Data, 12(1), 178, 2025.

- 433 Ministry of Economy, Trade, and Industry.: A survey on industry statistics.
- 434 https://www.meti.go.jp/statistics/tyo/kougyo/result-2/h10/kakuho/youti/youti1.html, 2007.
- 435 Ministry of Land, Infrastructure, Transport and Tourism.: Mesh Data of Subdivided Land Use in Urban Area.
- 436 https://nlftp.mlit.go.jp/ksj/gml/datalist/KsjTmplt-L03-b-u.html, 2021.
- 437 Morikawa M. Economies of density and productivity in service industries: An analysis of personal service industries based
- 438 on establishment-level data. Review of Economics and Statistics 93: 179–192, 2011.
- 439 Murakami, D., & Yamagata, Y.: Estimation of gridded population and GDP scenarios with spatially explicit statistical
- 440 downscaling. Sustainability, 11(7), 2106, 2019.
- 441 NESDC (Office of the National Economic and Social Development Council, Thailand).: Gross Provincial Product
- 442 1995–2009 (16 sectors). https://www.nesdc.go.th/main.php?filename=gross_regional, 2016.
- 443 Pesaresi M, Politis P.: GHS-BUILT-S R2022A: GHS built-up surface grid, derived from Sentinel2 composite and Landsat,
- 444 multitemporal (1975–2030). European Commission, Joint Research Centre (JRC), 2022.
- 445 Potapov P, Svetlana T, Matthew CH, Alexandra T, Viviana Z, Ahmad K, Xiao-Peng S, Amy P, Quan S, Jocelyn C.: Global
- 446 maps of cropland extent and change show accelerated cropland expansion in the twenty-first century. Nature Food 3: 19–28,
- **447** 2022.
- 448 Rose A.: Economic Principles, Issues, and Research Priorities in Hazard Loss Estimation. Modeling Spatial and Economic
- 449 Impacts of Disasters, Springer Berlin Heidelberg, Berlin, Heidelberg; 13-36, 2004.
- 450 Ru, Y., Blankespoor, B., Wood-Sichra, U., Thomas, T. S., You, L., & Kalvelagen, E.: Estimating local agricultural GDP
- 451 across the world. Earth System Science Data Discussions, 2022, 1-36, 2022.
- 452 Shoji T, Yamazaki D, Kita Y, Megumi W.: Global Sectoral GDP map at 30" resolution (SectGDP30) v1.0,
- 453 https://doi.org/10.5281/zenodo.13991673, 2024.
- 454 Sieg T, Thomas S, Kristin V, Reinhard M, Bruno M, Heidi K.: Integrated assessment of short-term direct and indirect
- 455 economic flood impacts including uncertainty quantification. PLOS ONE 14: e0212932, 2019.
- 456 Taguchi R, Tanoue M, Yamazaki D, Hirabayashi Y.: Global-scale assessment of economic losses caused by flood-related
- 457 business interruption. Water 14: 967, 2022.
- 458 Tanoue M, Hirabayashi Y, Ikeuchi H.: Global-scale river flood vulnerability in the last 50 years. Scientific Reports 6: 36021,
- **459** 2016.
- 460 Tanoue M, Taguchi R, Nakata S, Watanabe S, Fujimori S, Hirabayashi Y.: Estimation of direct and indirect economic losses
- 461 caused by a flood with long-lasting inundation: Application to the 2011 Thailand flood. Water Resources Research 56, 2020.
- 462 Tanoue M, Taguchi R, Alifu H, Hirabayashi Y.: Residual flood damage under intensive adaptation. Nature Climate Change
- **463** 11: 823-826, 2021.
- 464 Tellman B, Sullivan JA, Kuhn C, Kettner AJ, Doyle CS, Brakenridge GR, Erickson TA, Slayback DA.: Satellite imaging
- 465 reveals increased proportion of population exposed to floods. Nature 596: 80–86, 2021.

- 466 The European Environmental Agency.: CORINE Land Cover.
- 467 https://land.copernicus.eu/en/products/corine-land-cover?tab=main, 2017.
- 468 Theobald DM.: Development and Applications of a Comprehensive Land Use Classification and Map for the US. PLoS
- 469 ONE 9: e94628, 2014.
- 470 Wenz L, Carr RD, Kögel N, Kotz M, Kalkuhl M.: DOSE Global data set of reported sub-national economic output. Sci
- **471** Data 10: 425, 2023.
- 472 Wenz L, Willner SN.: 18. Climate impacts and global supply chains: An overview. Handbook on Trade Policy and Climate
- 473 Change, 290, 2022.
- 474 Willner SN, Otto C, Levermann A.: Global economic response to river floods. Nature Climate Change 8: 594–98, 2018.
- 475 The World Bank.: 2011 Thailand Floods: Rapid Assessment for Resilient Recovery and Reconstruction Planning.
- 476 https://recovery.preventionweb.net/publication/2011-thailand-floods-rapid-assessment-resilient-recovery-and-reconstruction-
- 477 planning, 2011.
- 478 The World Bank.: World Development Indicators. https://databank.worldbank.org/source/world-development-indicators,
- **479** 2023.
- 480 Yamazaki, D, Kanae S, Kim H, Oki T.: A physically-based description of floodplain inundation dynamics in a global river
- 481 routing model: FLOODPLAIN INUNDATION DYNAMICS. Water Resources Research 47: w04501, 2011.
- 482 Zhuang, L., & Ye, C.: More sprawl than agglomeration: The multi-scale spatial patterns and industrial characteristics of
- 483 varied development zones in China. Cities, 140, 104406, 2023